RR Pic (1925): A Chandra X-ray View

Y. Pekön* and S. Balman†

Department of Physics, Middle East Technical University, Inönü Bulvarı, Ankara, 06531, Turkey

14 December 2018

ABSTRACT

We present the Chandra ACIS-S3 data of the old classical nova RR Pic (1925). The source has a count rate of $0.067\pm0.002~c~s^{-1}$ in the 0.3-5.0 keV energy range. We detect the orbital period of the underlying binary system in the X-ray wavelengths. We also find that the neutral Hydrogen column density differs for orbital minimum and orbital maximum spectra with values $(0.25^{+0.23}_{-0.18})\times10^{22}~cm^{-2}$ and $(0.64^{+0.13}_{-0.14})\times10^{22}~cm^{-2}$ at 3σ confidence level. The X-ray spectrum of RR Pic can be represented by a composite model of bremsstrahlung with a photoelectric absorption, two absorption lines centered around 1.1-1.4 keV and 5 Gaussian lines centered at emission lines around 0.3-1.1 keV corresponding to various transitions of S, N, O, C, Ne and Fe . The bremsstrahlung temperature derived from the fits range from 0.99 to 1.60 keV and the unabsorbed X-ray flux is found to be $(2.5^{+0.4}_{-1.2})\times10^{-13}$ erg cm $^{-2}$ s $^{-1}$ in the 0.3-5.0 keV range with a luminosity of $(1.1\pm0.2)\times10^{31}$ erg s $^{-1}$ at 600 pc. We also detect excess emission in the spectrum possibly originating from the reverse shock in the ejecta. A fit with a cooling flow plasma emission model show enhanced abundances of He, C, N, O and Ne in the X-ray emitting region indicating existence of diffusive mixing.

Key words: binaries:close - Stars: individual: RR Pic - novae, cataclysmic variables - stars:rotation - white dwarfs - X-rays: stars

1 INTRODUCTION

Cataclysmic Variables (CVs) are interacting binary systems hosting a main-sequence secondary (sometimes a slightly evolved star) and a primary component, a white dwarf (WD) (Warner 1995). The accretion process occurs mainly through an accretion disc in cases where the WD does not have substantial magnetic field to channel the accretion flow onto the WD via the field lines. These systems are typically categorized by their eruptive behavior like Classical Novae, Recurrent Novae and Dwarf Novae (Z Cam type, U Gem Type, SU UMa type etc). In nonmagnetic systems X-rays are produced in the shocks at the inner disc boundary layer (Patterson & Raymond 1985; Verbunt et al. 1997; Baskill, Wheatley & Osborne 2005). These systems show hard X-ray spectra with 3-10 keV temperatures. In magnetic CV systems (mCVs) accreting matter is funneled by the magnetic field of the WD onto the magnetic poles forming a strong shock. The mCVs are classified into two categories where synchronized/almost synchronized systems are called Polars (Cropper 1990; Ramsay & Cropper 2004) with magnetic fields

in a range of 10-530 MG, these systems are characterized as being discless. The spectra of Polars may show the hot (above 10 keV temperature) hard X-ray tails if the accreting flow is dense and the magnetic fields are low ($\sim\!10^{-(10-11)}~\rm M_{\odot}~\rm yr^{-1})$ whereas more rarified streams and stronger magnetic fields favor cyclotron cooling where the hard X-ray tails are suppressed. Soft X-ray emission (via reprocessing) is enhanced once the accretion rate is $\geqslant\!10^{-9}~\rm M_{\odot}~\rm yr^{-1}$ (Schmidt et al. 2005). Highly asynchronous systems are called Intermediate Polars (Patterson 1994; Hellier 1996; Norton, Wynn & Somerscales 2004 and references therein) with magnetic fields in a range less than 10 MG where a truncated disc exists. These systems show hard X-ray bremsstrahlung spectra with 10-30 keV temperatures.

Classical nova RR Pic had an outburst in 1925 as a slow nova (expansion speed $\sim 400~\rm km~s^{-1})$. The shell shows "equatorial ring and polar cap/blob" geometry. There are similarities and important differences between the spectra in the ring and blob regions (in C and O lines) with a shell size of 30''x21'' and expansion rate of 850 km s $^{-1}$ for the ring (Gill & O'Brien 1998). The distance of the nova is measured to be $600\pm60~\rm pc$ (Gill & O'Brien 1998).

The point source RR Pic has an orbital period of $P_{orb} \sim 0.^d 14502545(7)$ (Kubiak 1984). A different periodicity of 15

 $^{^{\}star} \ \, \text{E-mail:yakup@astroa.physics.metu.edu.tr}$

[†] E-mail:solen@astroa.physics.metu.edu.tr

min is detected by Kubiak (1984) and accounted for the white dwarf period; hence making the source a candidate for intermediate polars. However, Haefner and Schoembs (1985) could not find the 15 min period with high-resolution photometry and concluded that the 15 min period is a transient event in the disc rather than the period of the white dwarf. Warner (1986) also confirms the absence of this 15 min period. Additionally he also finds flickering activity independent of the orbital phase coming from the disc itself rather than the hot spot and the system. Another period of 0.1577 days is also found interpreted as the superhump period of the system (Schmidtobreick et al. 2006). Furthermore, the source has a hardness ratio similar to Polars and the source spectrum in general differs compared with the non-magnetic CVs (van Teeseling, Beuermann & Verbunt 1996). Polarization measurements indicate the existence of two components of emission, one associated with a hot spot in the disc and the other in the preceding side of the disc opposite of the hot spot (Haefner & Metz 1982). Kubiak (1984) stated that the main optical light source in the system and the optical eclipse is due to the eclipse of the hot spot by the secondary. However, Schmidtobreick, Tappert & Saviane (2003) conclude that the eclipse is due to occultation of the emission from the preceding side rather than the hot spot.

2 OBSERVATION AND DATA

RR Pic and its vicinity was observed using the Chandra (Weisskopf, O'dell & van Speybroeck) Advanced CCD Imaging Spectrometer (ACIS; Garmire et al. 2003) for a 25 ksec on 2001 October 30 (PI=S. Balman), pointed at the nominal point on S3 (the back-illuminated CCD) with no gratings in use yielding a moderate non-dispersive energy resolution. The data were obtained at the FAINT mode. Chandra has two focal-plane cameras and two sets of transmission gratings that can be inserted in the optical path (HETG and LETG; High and Low Energy Transmission Gratings). The ACIS is used either to take high resolution images with moderate spectral resolution or is used as a read out device for the transmission gratings. ACIS is comprised of two CCD arrays, a 4-chip array, ACIS-I; and a 6-chip array, ACIS-S. The ACIS-S3 has a moderate spectral resolution $E/\Delta E \sim$ 10-30 (falls to about 7 below 1 keV) with an unprecedented angular resolution of 0.49" per pixel (half-power diameter). The standard pipeline processing was done by CXC. For the spectral and temporal analysis of the data we used the software packages CIAO 3.2 (Fruscione et al. 2006), XSPEC 12.2.1 and XRONOS 5.21 (Arnaud 1996; Blackburn 1995). For spectral analysis, background subtracted spectrum was created using the CIAO tools and the spectrum was binned such that each bin contained data with signal-to-noise ratio higher than 3. The data were then fitted with XSPEC. In general, data bins below 0.3 keV and above 5.0 keV were omitted due to low statistical quality. For the timing analysis, data times were barycentrically corrected and a background subtracted light curve was extracted using CIAO. The light curve was then folded. The phase resolved spectroscopy was performed by extracting spectra using the appropriate phases with the Chandra tools, then fitted using XSPEC. We also used CIAO 4.0 Beta 2 version and performed ACISprocessevents and checked if differences in spectra and light curve existed. We found no significant changes in the results.

The original observation of RR Pic was conducted in order to search for the extended emission from the old nova shell in accordance with the X-ray remnant of the old nova GK Persei (Balman 2005). Balman (2006) show that an extended emission is marginally detected in a short exposure with a count rate of 0.0023 c s^{-1} above the background as an elongated region extending from N to S about ± 19 arcsec. The elongation in the *Chandra* image is in agreement with the orientation of the equatorial ring in the H_{α} image. Images can be found in Balman (2006) and some preliminary analysis of the *Chandra* observation of RR Pic is in Balman and Küpcü-Yoldaş (2004).

3 THE Chandra SPECTRUM OF THE POINT SOURCE

The Chandra spectrum of the source can not be fitted by a single or two-temperature bremsstrahlung model including neutral Hydrogen absorption (phabs, wabs (models in XSPEC)) with a reduced χ^2 value smaller than 2. A fit with a single bremsstrahlung model is presented in Figure 1a. The fit doesn't actually reflect the features of the spectrum properly, leaving a hard excess above 2 keV. Moreover, the residuals of the fit in Figure 1a are scattered around the mean up to 4σ in the 0.5-2 keV region. To reduce the scattering of the residuals we added two absorption lines to the bremsstrahlung model around 1.15 and 1.25 which improved the fit diminishing the reduced χ^2 down to 1.75 but still maintaining the scattering around 0.5-1 keV and the hard excess (see Figure 1b). Thus, we concluded that there are line contributions to the continuum in the 0.5-1 keV energy range. Including emission lines to the fit both reduced the hard excess and the scattering of the data as well as improving the reduced χ^2 to 1.13.

Therefore a proper fit is with a composite model of bremsstrahlung together with a model of photoelectric absorption of HI, two absorption lines around 1.1-1.4 keV and 5 Gaussians centered on the likely emission lines around 0.3-1.1 keV energies. The fit is shown in Figure 1c and spectral parameters are shown in Table 1. The Gaussian lines fitted to the spectrum correspond to a range of emission lines of Fe (transitions between XVII and XXIV), S (XIV and XVI), Ca (transitions between XV and XVII), Ne (IX, X), O (VII, VIII), C VI. The absorption lines correspond to Fe (transitions between XVII and XXIV), Ne (X, IX) and Na X. However, due to the spectral resolution limitations of ACIS-S, the precise energy of the emission lines and absorption lines cannot be determined.

According to Mukai et al. (2003) X-ray spectra of CVs can be categorized as being of a cooling flow plasma emission model or of a photoionized plasma emission model. The source spectrum can not be fit with the photoionization model *photoion* ¹ so the shocked plasma emission can be inferred to be a cooling flow gas as in other nonmagnetic

 $^{^{1} \ \} See \ http://heasarc.gsfc.nasa.gov/docs/xanadu/xspec/models/photoion.html}$

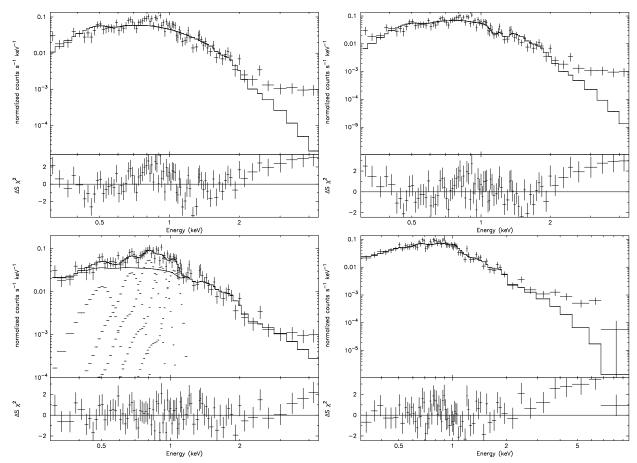


Figure 1. Various spectral fits to the RR Pic data in the 0.3-5 keV range. The crosses show the data with error bars, solid lines the composite fitted model and the dashed lines show the individual models. The panels under the spectra show residuals in standard deviations. The models fitted to the spectra are as follows: a) Simple Bremsstrahlung, top left-hand side panel b) Bremsstrahlung with 2 absorption lines, top right-hand side panel c) Bremsstrahlung with 2 absorption and 5 emission lines, bottom left-hand side panel and d) VMCFLOW, bottom right-hand side panel.

CVs V603 Aql, U Gem and SS Cyg (Mukai et al. 2003). Therefore, we fitted the spectrum with a cooling flow emission model with variable abundances such as VMCFLOW (Mushotzky & Szymkowiak 1988). The model fits the spectrum well with a reduced χ^2 of 1.58 showing increased abundance ratios of He, C, N and O with respect to solar (see Figure 1f for the fit and Table 1 for the spectral parameters).

Adding a blackbody component along with the bremsstrahlung or other plasma models as suggested by van Teeseling et. al. (1996) improves the fits; however the blackbody temperature derived from the fits are around 0.4-0.7 keV which is too high for any physical interpretation. The blackbody temperature should be in a range 0.01-0.06 keV for mCVs (e.g. Evans & Hellier 2007). Also, such a range of blackbody temperatures are not typical of nonmagnetic CVs (Baskill et al. 2005).

4 TEMPORAL ANALYSIS OF THE POINT SOURCE

The background subtracted light curve extraction of the source was done by the standard CIAO ACIS light curve extraction procedures. Plotting and epoch folding were performed with XRONOS 5.21.

Figure 2a shows background subtracted time series with bin time of 1100 s. The X-ray light curve of the source shows variation when folded on the orbital period of the system, 12528 s (0.14502545(7) d) which is shown in Figure 2b. The light curve in Figure 2a has been used for the folding process. The ephemeris of the radial velocities from Schmidtobreick et al. (2003) was used (HJD $_{start}=2452328.578335+0.14502545E)$ in the folding process. A simple sinusoidal fit to the folded light curve yields an X-ray modulation amplitude of 0.02 $c\ s^{-1}$ with 33% statistical error.

We performed orbital phase resolved spectroscopy of the source by extracting phases between 0-0.2 for the maxima and 0.3-0.45 for the minima. Figure 3a shows the fit to the maximum spectrum and 3b the minimum spectrum using a model with a single bremsstrahlung together with a model for photoelectric absorption of HI. The gaussian absorption and emission lines used in the entire spectrum were not used in these spectra. The low statistical quality of the minimum and maximum phase spectra does not allow the detection of lines. The spectral parameters are given in Table 2. The fits show a difference in the column density of neutral Hydrogen absorption between minimum and maximum spectrum in the 3σ confidence range.

4 Pekön Y. and Balman, Ş.

Table 1. Spectral parameters of the entire spectrum of the RR Pic in the energy range 0.3-5 keV. N_H is the absorbing column; kT_{Bremss} is the bremsstrahlung temperature; LowT and HighT are low and high temperature values for VMCFLOW; He, C, N, O, Ne are the abundance ratios with respect to the solar abundances; Gabs LineE is the absorption line centers for the absorption lines, (the sigma and Tau parameters are frozen at 0.005 and 50 for the first line and 0.01 and 20 for the second line), Gaussian LineE is the line center for the emission lines (the sigma values for the lines are frozen at 0.001); K_{Bremss} , $K_{VMCFLOW}$ and K_G are the normalizations for the bremsstrahlung, VMCFLOW and Gaussian models respectively. The fluxes are given for the entire model in the first row and then for each of the components in the following rows. All error ranges are given in %90 confidence level ($\Delta \chi^2$ =2.71 for a single parameter)

	BREMSS+2ABS+5GAUSS	VMCFLOW
$N_H \ (\times \ 10^{22} \ \text{atoms/cm}^2)$	$0.008^{+0.014}_{>}$	$0.008^{+0.008}_{-0.007}$
kT_{Bremss} (keV)	$1.3^{+0.3}_{-0.3}$	N/A1
LowT (keV)	N/A	$0.14^{+0.10}_{>0.02}$
HighT (keV)	N/A	$1.8^{+0.2}_{-0.2}$
K_{Bremss}	$0.00097^{+0.00003}_{-0.00002}$	N/A
$K_{VMCFLOW}~(\times~10^{-9})$	N/A	$1.8^{+0.1}_{-0.1}$
Не	N/A	40.4±9.1
\mathbf{C}	N/A	$18.4^{+6.1}_{-6.1}$ $1.7^{+16.5}_{-8.7+7.1}$
N	N/A	0.1
O	N/A	$1.9_{-0.7}^{+1.1}$
Ne	N/A	1 (frozen)
Gabs LineE (keV)	A1: $1.14^{+0.03}_{-0.02}$	N/A
	A1: 1.14_0.02 A2: 1.28+0.02 A2: 1.20+0.02	
Gaussian LineE (keV)	G1: $0.53^{+0.03}_{-0.09}$	N/A
	G2: $0.66^{+0.04}_{-0.02}$	
	G3: $0.80^{+0.02}_{-0.02}$	
	G4: $0.90^{+0.02}_{-0.02}$	
	G5: $1.02_{-0.02}^{+0.02}$	
$K_G \ (\times \ 10^{-6})$	G1: $7.3_{-5.1}^{+4.4}$	N/A
	G2: $9.4_{-4.1}^{+4.1}$	
	G3: 14^{+2}_{-4}	
	G4: $8.4^{+2.8}_{-2.4}$	
	G5: $6.2^{+\overline{1.9}}_{-2.0}$	
Flux (× 10^{-13} ergs/cm ² /s)	$2.5^{+0.4}_{-1.2}$	$2.2^{+0.3}_{-0.6}$
	Bremss: $0.4_{-0.28}^{+0.46}$	
	G1: $0.07_{-0.06}^{+0.09}$	
	G2: $0.11^{+0.08}_{-0.09}$	
	G3: $0.19^{+0.06}_{>}$	
	G4: $0.13_{-0.07}^{+0.08}$	
	G5: $0.11^{+0.10}_{-0.08}$	
$\chi^2_{ u}$	1.13 (73 d.o.f.)	1.58 (66 d.o.f)

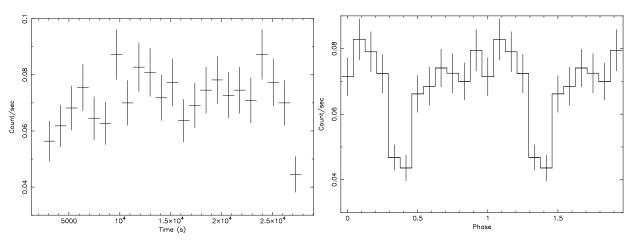


Figure 2. Left-hand panel is the light curve of RR Pic with a bin time of 1100 s. Right-hand panel is the light curve of RR Pic folded over the orbital period of 0.145025 days.

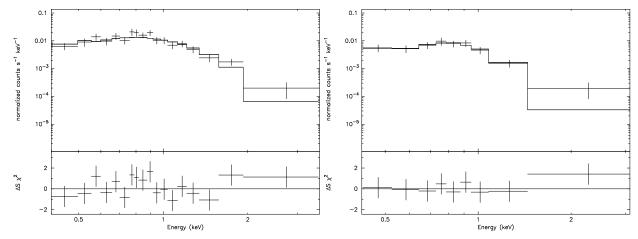


Figure 3. The spectra of orbital phase maximum on the right-hand panel and minimum on the left. Both spectra were fitted with a model of bremsstrahlung and photoelectric absorption of HI. The crosses show the data with error bars and solid lines show the composite fitted model. The panels under the spectra show residuals in standard deviations.

Table 2. Spectral parameters of maximum and minimum spectra in the 0.3-5 keV region. Both spectra were fitted with a model of bremsstrahlung and photoelectric absorption of HI. N_H is the absorbing column, kT_{Bremss} is the bremsstrahlung temperature and K_{Bremss} is the bremsstrahlung normalization. Error ranges for kT_{Bremss} and K_{Bremss} correspond to 2σ confidence level, error range for N_H correspond to 3σ confidence level.

	Maxima	Minima
$N_H (\times 10^{22} \text{ atoms/cm}^2)$ $kT_{Bremss} \text{ (keV)}$ K_{Bremss} χ^2_{ν}	$\begin{array}{c} 0.25^{+0.23}_{-0.18} \\ 0.35^{+0.2}_{-0.13} \\ 0.0004^{+0.0028}_{>} \\ 1.05 \; (15 \; \mathrm{d.o.f.}) \end{array}$	$\begin{array}{c} 0.64^{+0.14}_{-0.13} \\ 0.14^{+0.21}_{-0.04} \\ 0.03^{<}_{-0.03} \\ 0.49 \text{ (6 d.o.f.)} \end{array}$

5 DISCUSSION

The Chandra ACIS-S spectrum of RR Pic fits well with two spectral models. First one is a composite model of single bremsstrahlung, photoelectric absorption, two absorption lines and 5 Gaussian lines at 2-3 σ confidence level. Another good fit is with VMCFLOW model with enhanced abundances of He, C, N, O and Ne. The good fitting models are consistent with each other since the Gaussian lines of the composite model are also in accordance with the abundances of VMCFLOW.

The X-ray luminosity can be calculated as $(1.1\pm0.2)\times10^{31}$ erg s⁻¹ (using the relation L= $4\pi d^2F$). Assuming the accretion luminosity is half the total luminosity; taking the mass and the radius of the white dwarf to be 1 M_{\odot} and 10⁹ cm, respectively; the accretion rate \dot{M} is 1.7×10^{14} g s⁻¹ (using the relation L=G \dot{M} M/2R). These values are consistent with those of the nonmagnetic CVs in quiescent state (Baskill et al. 2005).

The fit residuals, in general, show some excess (particularly with VMCFLOW model) on the harder energy part of the spectrum. In order to understand the nature of the excess, spatially resolved spectra around the position of the source was extracted from the south-southeast and north-northwest regions of the source in accordance with the results of Balman 2002 and 2006. Both regions fit well with the composite model noted in Table 1 of bremsstrahlung and

emission lines. However, a 2-3 σ hard excess in the southsoutheast region needs an additional bremsstrahlung component to be added to decrease the reduced χ^2 values down to desirable levels below 2. This component has very high absorption around 50×10^{22} cm⁻² and plasma temperature in a range 0.36-0.70 keV. This excess emission can be attributed to emission from the shocked nova shell. In order to investigate this using the Rankine-Hugoniot jump conditions one can derive a relation between the post-shock temperature and expansion speed of the material (nova ejecta or the ring) as $kT_{shock} = (3/16)\mu m_H (v_{shell})^2$. Taking v_{shell} as $400-850~{\rm km~s^{-1}}$ range for RR Pic (see Introduction), the shocked nova shell temperature is 0.31-1.4 keV consistent with our derived fit result suggesting a component from the nova shell. Moreover, the high absorption towards this component can be expected if it is of the reverse shock, high absorption in the reserve shock was also detected for the shell of GK Persei (Balman 2005).

The abundances of He, C, N and O derived from the fits to the source spectrum with the VMCFLOW model are significantly enhanced, where fits with solar abundances are ruled out with reduced χ^2 larger than 2. This means that the X-ray emitting region in the point source consists of enhanced abundances of these elements which can be explained by the mixing that has occurred in this system. Prior to the thermonuclear runaway in a classical nova explosion, diffusion by convection takes place between the hydrogen rich boundary layer and the white dwarf where heavier elements such as He, C, N and O are present (Livio 1994). Hence, as heavier elements diffuse into the boundary layer, the abundances are increased. What we observe in the spectrum of RR Pic can be a very rare example of diffusive mixing in a Classical Nova.

The light curve of the source shows variation folded on the orbital period with a modulation amplitude of 0.02 counts s⁻¹ with %33 statistical error. Comparing the spectra of the orbital maximum and minimum of the source reveals that the X-ray modulation could be due to the change in the difference in photoelectric absorption between the two phases. In order to explain this, an analogy to the Low Mass X-ray Binaries (LMXBs) can be used. In some LMXBs, the

X-ray intensity shows dipping behaviour during the orbital motion, caused largely by the obscuration of the X-rays by the region where the accreting material impacts the disc (White & Swank 1982). Thus in our case, the X-ray modulation can be due to the obscuration by a warm/cold region on the disc, similar to LMXBs. As Parker, Norton and Mukai (2005) states, a similar orbital modulation is also present in some CVs. Their work suggests that decrease of modulation depth with increasing energy implies photoelectric absorption due to material at the edge of the disc for the systems they have studied. Furthermore, according to the doppler tomography analysis of RR Pic by Schmidtobreick et al. (2003), a strong emission region is detected at phase 0.3 opposite the bright hot spot (i.e., accretion impact region). Using their radial velocity ephemeris, we find that the X-ray eclipse/dip corresponds to the same orbital phase 0.3. Therefore this supports the idea that the X-ray modulation is due to an absorbing region on the disc.

The two absorption features that are detected in the spectrum of RR Pic around 1.1-1.2 keV are not accounted for before in any CV. We also checked the data against any instrumental feature or processing differences between software versions and the features are persistent. They can be fitted with absorption lines corresponding to Ne IX and Fe (transitions between XVII–XXII) for the first, and Ne X and Fe (transitions between XIV–XXVI) for the second feature. These features could be caused by a region on the disc or the shell itself in the line of sight. Further investigation of the spectrum could prove useful in finding the origin of these features.

6 SUMMARY AND CONCLUSIONS

We present the first broad X-ray spectrum of RR Pic in the 0.2-10.0 keV range using Chandra ACIS-S3 observations.

The spectrum of the source shows a bremsstrahlung temperature in the range 1-1.6 keV that is consistent with the temperature range of the non-magnetic CVs of 1-5 keV (Kuulkers et. al 2006). Emission lines of the elements Fe (transitions between XVII and XXIV, (Fe L complex)), S (XIV and XVI), Ca (transitions between XV and XVII), Ne (IX, X), O (VII, VIII), C VI; and absorption lines of elements Fe (transitions between XVII and XXIV), Ne (X, IX) and Na X are consistent with the spectrum. In order to determine the exact transitions of the emission and absorption lines, observations with higher sensitivity and resolution is needed.

The absorption features detected in the spectrum are particularly important since no absorption feature at these energies were detected before in any CV. So a secure detection/confirmation of the absorption lines would be a novel discovery if further observations are carried out.

The spectrum clearly fits well with VMCFLOW model rather than the *photoion* model which implies that the X-rays from the system arises from a shocked cooling flow plasma. From the VMCFLOW fit, we derive temperature range with high $T=1.8^{+0.2}_{-0.2}$ keV and low $T=0.14^{+0.10}_{>}$ keV. The fit also reveals high abundance ratios with respect to the solar abundances such as $18.4^{+9.1}_{-6.1}$, $1.7^{+16.5}_{>}$, $8.7^{+7.1}_{>}$ and $1.9^{+1.1}_{-0.6}$ for He, C, N and O respectively. These abundance enhancements indicate existing mixing in the boundary layer.

The high He and N abundances indicate Hydrogen burning which would be a consequent result of a nuclear burning stage of a classical nova explosion. So the spectrum of RR Pic demonstrates a very rare example of diffusive mixing prior to and after the thermonuclear runaway in a Classical Nova detected long years after the explosion. We also find excess emission in the spectra $(2-3\sigma)$ that we attribute the origin to be the shocked nova shell with a temperature of 0.3-0.7 keV.

We clearly detect the orbital modulation of RR Pic in the X-ray wavelengths. Using the ephemeris given by Schmidtobreick et al. (2003), the phase of the X-ray eclipse of the system overlaps with the phase of the emission region from the disc opposite of the bright spot. We also find that the neutral Hydrogen column density differs for orbital minimum and orbital maximum spectra with values $(0.25^{+0.23}_{-0.18})\times10^{22}~{\rm cm}^{-2}$ and $(0.64^{+0.13}_{-0.14})\times10^{22}~{\rm cm}^{-2}$ at 3σ confidence level. Therefore we favor a model where a possible warm/cold absorbing region on the disc or line of sight, the nova shell, modifying the spectrum.

ACKNOWLEDGMENTS

We thank the anonymous referee for critical reading of the manuscript.

YP acknowledge support from TÜBİTAK, The Scientific and Technological Research Council of Turkey, through project 106T040. SB acknowledges an ESA fellowship and also a TUBA-GEBIP fellowship from the Turkish Academy of Sciences.

REFERENCES

Arnaud K. A., 1996, in Jacoby G., Barnes J., eds, ASP Conf. Ser. Vol. 101, Astronomical Data Analysis Software and Systems V., Astron. Soc. Pac., San Francisco, p. 17

Balman S., 2006, AdSpR, 38, 2840

Balman Ş., 2005, ApJ, 627, 933

Balman Ş., Küpcü-Yoldaş A., 2004, in Vrielmann S., Cropper M., eds, IAU Colloq. 190: Magnetic Cataclysmic Variables, Astronomical Society of the Pacific Conference Series, vol. 315, 172

Balman Ş., 2002, in Hernanz M., and José J., eds, Classical Nova Explosions, American Institute of Physics Conference Series, vol. 637, 365

Baskill D.S., Wheatley P.J., Osborne J.P., 2005, MNRAS, 357, 626

Blackburn J. K., 1995, GeCoA, 59, 513

Cropper M., 1990, SSRv, 54, 195

Evans P. A., Hellier C., 2007, ApJ, 663, 1277

Fruscione A. et al., 2006, SPIE, 6270, 60

Garmire G. P., Bautz M. W., Ford P. G., Nousek J. A., Ricker G. R., 2003, SPIE, 4851, 28

Gill C. D., O'Brien T. J., 1998, MNRAS, 300, 221

Haefner R., Metz K., 1982, A&A, 109, 171

Haefner R., Schoembs R., 1985, A&A, 150, 325

Hellier C., 1996, in Evans A., Wood J.H., eds, Cataclysmic Variables and Related Objects, Kluwer Academic Publishers, Dordrecht, p. 143

Kubiak M., 1984, Acta Astron., 34, 331

Kuulkers E., Norton A., Schwope A., Warner B., 2006, in Lewin W., van der Klis M., eds, Compact stellar X-ray sources, Vol. 39, p. 421

- Livio M., 1994, in Nussbaumer H., Orr A., eds, Interacting Binaries, Springer, Berlin, p. 135
- Mukai K., Kinkhabwala A., Peterson J. R., Kahn S. M., Paerels F., 2003, ApJ, 586, L77
- Mushotzky R.F., Szymkowiak A.E., 1988, in Fabian A.C., eds, Cooling flows in clusters and galaxies, Kluwer, Dordrecht, p. 53
- Norton A. J., Wynn G. A., Somerscales R. V., 2004, ApJ, 614, 349
- Parker T. L., Norton A. J., Mukai K., 2005, A&A, 439, 213
- Patterson J., Raymond J. C. 1985, ApJ, 292, 535

Paterson J., 1994, PASP 106, 209

Ramsay G., Cropper, M., 2004, MNRAS, 347, 497

Schmidt G. D. et al., 2005, ApJ, 630, 1037

Schmidtobreick L., Tappert C., Ederoclite A., Saviane I., Mason E., 2006, Ap&SS, 304, 303

Schmidtobreick L., Tappert C., Saviane I., 2003, MNRAS, 342, 145

van Teeseling A., Beuermann K., Verbunt F., 1996, A&A, 315, 467

Verbunt F., Bunk W. H., Ritter H., Pfeffermann E., 1997, A&A, 327, 602

Warner B., 1995, Cataclysmic Variable Stars, Cambridge University Press, Cambridge

Warner B., 1986, MNRAS, 219, 751

Weisskopf M. C., O'dell S. L., van Speybroeck L. P., 1996, SPIE, 2805, 2

White N. E., Swank J. H., 1982, ApJ, 253, 61

This paper has been typeset from a TeX/ \LaTeX file prepared by the author.